# Nanostructured microtubes based on $TiO_2$ doped by Zr and Hf oxides with the anatase structure

**VV Zheleznov[1,*], EI Voit[1], YV Sushkov[1], SA Sarin[1], VG Kuryavyi[1], DP Opra[1], SV Gnedenkov[1], SL Sinebryukhov[1] and AA Sokolov[2]**
[1]Institute of Chemistry Russian Academy of Sciences Far Eastern-Branch, 159, Prosp. 100-letya Vladivostoka, Vladivostok 690022, Russia
[2]Far Eastern Federal University, 8, Sukhanova Str., Vladivostok 690950, Russia

[*]E-mail: zheleznov_sergey@mail.ru

**Abstract.** The nanostructured microtubes based on $TiO_2$ have been prepared on the carbon fiber template using the sol-gel method. The microtubes consist of nanoparticles of metal oxides: $TiO_2/ZrO_2$ and $TiO_2/HfO_2$. The dependence of microtubes morphology and nanoparticles structure on the synthesis conditions has been studied using the methods of SEM, SAXS, and Raman spectroscopy. It has been demonstrated that at the stoichiometric ratio of up to 0.04 for Zr/Ti and up to 0.06 for Hf/Ti microtubes consist of uniform nanoparticles with the anatase structure. Along with further increase of the dopants content in the microtubes composition, nanoparticles acquire the core-shell structure. It has been suggested that nanoparticles have a core composed of the solid solutions $Ti_{1-x}Zr_xO_2$ or $Ti_{1-x}Hf_xO_2$ and a shell consisting of zirconium or hafnium titanate. The fabricated Zr- and Hf-doped $TiO_2$ materials were investigated in view of their possible use as anode materials for Li-ion batteries. Charge–discharge measurements showed that the doped samples manifested significantly higher reversibility in comparison with the undoped $TiO_2$. The method opens new prospects in synthesis of nanostructured materials for Li-ion batteries application.

## 1. Introduction

Recently times, a substantial attention has been paid to nanosized titanium and zirconium dioxides. The applications of these materials in the industry are diverse and include many branches: production of pigments for paint-and-varnish industry, manufacture of catalysts and their substrates, fabrication of glass, ceramics and refractory materials, electrical engineering, and photocatalysis [[1], [2], [3]]. The fabrication of modified forms of $TiO_2$ substantially extends the range of application of these materials [[4], [5]].

Up to present, many methods of synthesis of highly disperse materials based on titanium dioxides have been developed [[2], [6],[7],[8]]. One of the well-known methods of fabrication of nanosized oxides is the sol-gel technique including a number of consecutive stages: preparation of the precursor solution, sequential transformation of it into sol and, thereafter, into gel (as a result of hydrolysis and condensation processes), drying, and thermal treatment. The advantages of the sol-gel technique consist in the possibility to produce nanoparticles of multi-component oxides with high degree of chemical homogeneity and to change the nanoparticles phase composition, size, and shape. The main disadvantage of the synthesis method is related to the loss of control over the nanoparticles size and shape during gel drying and thermal treatment [[2]].

In the present paper, the nanostructured oxide microtubes of the composition $TiO_2/ZrO_2$ and $TiO_2/HfO_2$ have been prepared by means of the of template sol-gel method. The relationship between the morphology, structure, and synthesis conditions of the materials was studied. The possibility of application of the syntehsized $TiO_2$-based microtubes as anodes for Li-batteries was discussed.

## 2. Synthesis of materials and methods of study

### *2.1. Synthesis*

The scheme of synthesis is shown in Figure 1. The method of fabricating the microtubes is based on a slow hydrolysis in aqueous solutions of the inorganic precursors of titanium, zirconium, and hafnium accompanied with deposition of oxides on the template surface [[9]]. In the synthesis process, the following precursors were used: $TiCl_4$, $ZrOCl_2$, and $HfOCl_2$. Busofit T055 carbon fiber manufactured at the Belogorsk Chemical Fibers Plant (Belarus) was used as a template. The specific surface of the carbon fiber was determined using an ASAP 2020 V3.04 H (Micrometrics, USA) spectrometer from isotherms of low-molecular adsorption of nitrogen by the BET method: it was equal to 960 $m^2 g^{-1}$. The porosity distribution was evaluated using the original density functional theory (DFT). The major part of the surface (780 $m^2 g^{-1}$) is formed d by micropores of a diameter of 2 nm. The template removal was carried out through slow annealing at a temperature of 500°C in air. The carbon template annealing was controlled using Raman spectroscopy. In the course of the extra thermal treatment at 550–850°C in air for 30 min, nanocrystallization of oxide tubes structural units was observed. Since the initial carbon fiber contains ~0.01 wt. % of silicon, some amount of $SiO_2$ is always present in the materials. The decrease of the $SiO_2$ concentration in the sample was achieved through autoclave pretreatment of the initial template by ammonium bifluoride. In the samples of as-prepared materials, the $SiO_2$ content was about 2-5 wt. %. The effect of the $SiO_2$ content in the above range on the microtube structure and morphology has not been identified. The proposed synthesis technique allows regulating over a broad range the phase composition, size, and shape of the nanostructural units by changing the synthesis conditions (solution pH, component concentrations, and annealing temperature).

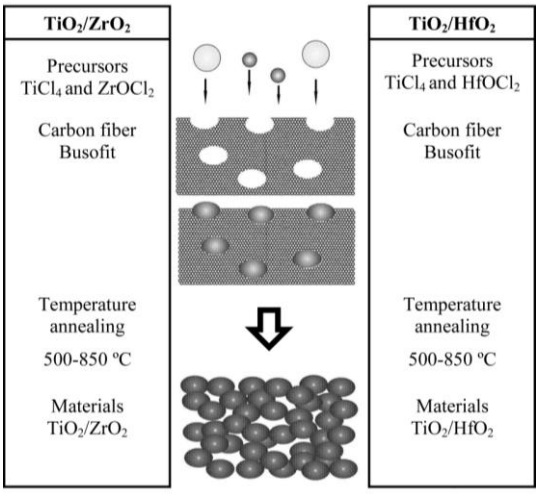


**Figure 1.** Synthesis scheme for nanosized oxide microtubes.

### *2.2. Methods of study*

The content of titanium, zirconium, hafnium, and silicon oxides in the materials was determined by the energy-dispersive X-ray analysis on an EDX 700 (Shimadzu, Japan) spectrometer. The morphology was investigated by the method of scanning electron microscopy (SEM) using high-resolution S5500

and TEM-3000 (Hitachi, Japan) microscopes. The sizes of microtubes nanoparticles were determined by the method of small angel X-Ray scattering (SAXS). The measurements were carried out on an S3-MicroPIX (Hecus X-ray systems, Austria) spectrometer connected to a Xenocs GeniX generator (France) operated at 50 kV and 1 mA with using CuKα radiation (λ = 0.154 nm).

The Raman spectroscopy method was used to determine more accurately the structure and structural effects of separate components in the obtained material. The registration of the spectra was carried out on an RFS-100/S Fourier-Raman spectrometer (Bruker, Germany) with high-sensitive germanium detector. The Nd:YAG laser with the wavelength of 1064 nm was used as the excitation source.

The working electrode consisted of the active material, carbon black, and polyvinylidene fluoride binder at a weight ratio of 80 : 10 : 10. A lithium metal disc was applied as both counter and reference electrodes. 1 M solution of $LiBF_4$ salt in the mixture of propylene carbonate and dimethoxyethane at a volume ratio of 3:1 was used as an electrolyte. The design of the electrochemical half-cell is described in detail in [[10],[11],[12]]. The electrochemical performance was evaluated using a Solartron 1470E (UK) potentiostat/galvanostat. The parameters were measured by the galvanostatic discharge–charge at a current rate of 0.1*C* ($C$ = 335 mAh $g^{-1}$) in the range from 3 to 1 V during 20 cycles. Within the scopes of the present work, due to half-cell applying, the lithiation process corresponds to discharge while the delithiation – to charge.

## 3. Discussion of results

### *3.1. Morphology*

The morphology study by the SEM method demonstrated that all the fabricated materials consist of microtubes (Figure 2).

The diameters of oxide tubes vary from 1 to 5 μm, their lengths – from 10 to 100 μm, whereas the tube wall thicknesses change in the range of 100 to 500 nm. The microtubes are composed of nanoparticles of sizes from 15 to 50 nm.

The lengths, external and internal diameters, and porosity of microtubes as well as the nanoparticle sizes depend on the content of dopants and treatment temperature. Along with increase of the content of dopants and treatment temperature increase from 550C to 850°C, the decrease in the oxide microtubes lengths was observed and the degree of their destruction increased. One can see that $TiO_2/ZrO_2$ microtubes are characterized by a lesser diameter than $TiO_2/HfO_2$ ones.

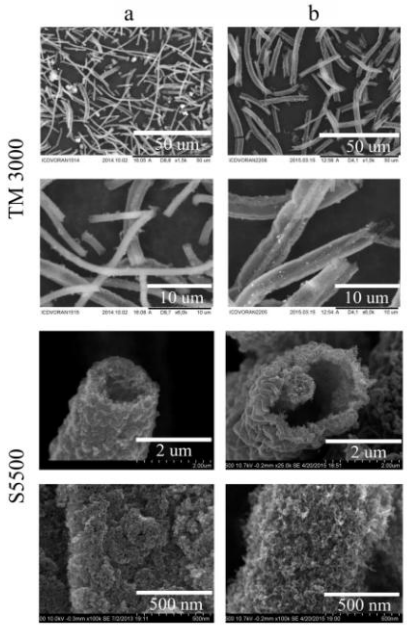


**Figure 2.** SEM micrographs of the $TiO_2/ZrO_2$ (a) and $TiO_2/HfO_2$ (b) obtained on S5500 and TM-3000 microscopes.

### *3.2. Nanoparticle sizes*

To estimate the sizes of nanoparticles forming the tubes, the SAXS method was used. Based on the SAXS spectra, the pair distribution functions *P(r)* of the radii of gyration for scattering particles ($R_g$) were calculated, which allowed revealing the regularities in the arrangement of neighboring atoms, molecules, or atomic groups at a distance of *r*. The program GNOM was used [[13]]. The obtained *P(r)* and $R_g$ for the materials are presented in Figures 3, 4.

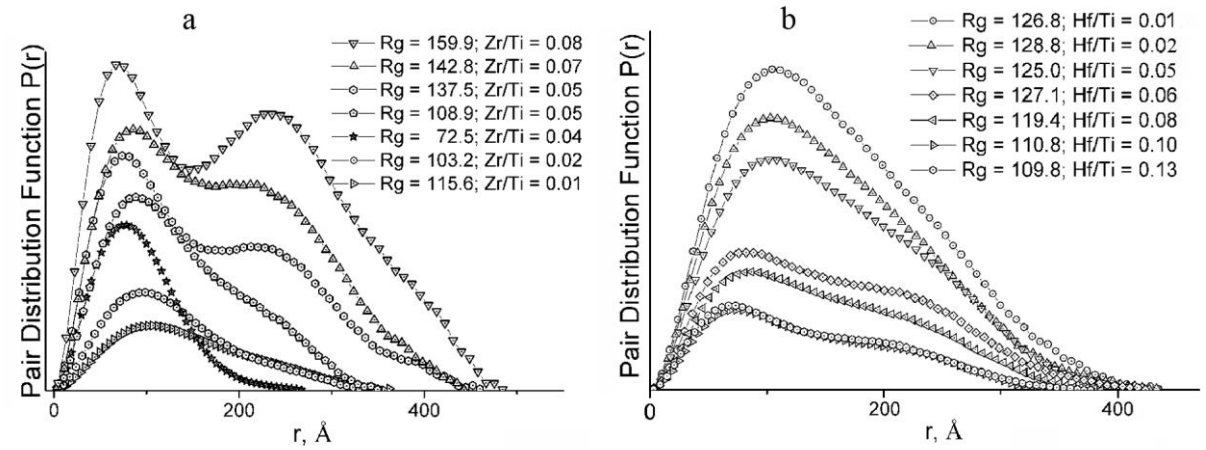


**Figure 3.** Dependence of pair distribution functions on the particles radius.

For Zr-doped microtubes, the type of *P(r)* curve corresponds to scattering from spheroids at Zr/Ti ratio of lower than 0.04 (doping level) (Figure 3a). In this concentration range, *P(r)* has one maximum. The dependence of $R_g$ for nanoparticles on the Zr/Ti ratio shows that the average sizes of nanoparticles decrease nonlinearly (Figure 4). The decrease in average sizes of nanoparticles is probably related to the increase in heterogeneity of the nanoparticles' crystalline lattice and growing microstress in them due to dopant inclusion [[14]]. The calculated maximal diameters of the scattering particles vary from 25 to 35 nm (Figure 3a).

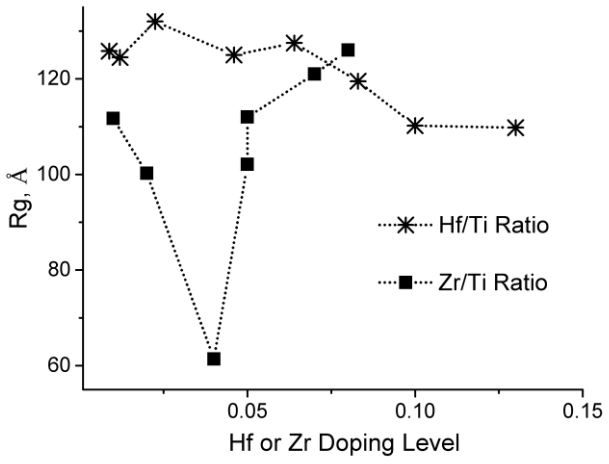


**Figure 4.** Dependence of the average inertia radius of the nanoparticles on the doping level.

If the Zr/Ti ratio is higher than 0.04, the second maximum increasing along with the increase of the $ZrO_2$ content emerges on the *P(r)* curve while $R_g$ of nanoparticles increases. As was found earlier, the binary form of the *P(r)* curve corresponded to the formation of nanoparticles with the core-shell

structure [[13], [15]]; in this case, the nanoparticle comprises a shelled nanocrystallite. The calculated maximal diameter of scattering particles varies in the range from 35 to 50 nm depending on the doping level (Figure 3b).

The character of changes in the sizes of nanoparticles forming the basis of Hf-doped microtubes differs from that of Zr-doped ones. At the annealing temperatures of 650°C and the doping level of up to 0.06, the average sizes of particles do not virtually change being equal to about 25 nm (Figure 4). Further increase of the Hf/Ti ratio results in the decrease in the nanoparticles sizes and the emergence of the second maximum on the *P(r)* curve (Figure 3b).

*3.3. Structure of nanoparticles*

To determine the structure of nanoparticles forming the microtubes and reveal the role of dopants in the synthesized materials, their Raman spectra were studied. Raman spectroscopy is known to enable one to identify changes in the matter crystalline state even if the particle sizes are small.

As was established earlier that in the Raman spectrum of the polycrystalline $TiO_2$ with the structure of anatase at the room temperature in accordance with the data of the factor-group analysis $\Gamma(D_{4h}^{19}) = 1A_{1g}(\text{Raman})+1A_{2u}(\text{IR})+2B_{1g}(\text{Raman})+1B_{2u}+3E_g(\text{Raman})+2E_u(\text{IR})$, six modes are active: $\nu_1+\nu_3$=515 $cm^{-1}$ ($A_{1g}$, $B_{1g}$), $\nu_4$=396 $cm^{-1}$ ($B_{1g}$), $\nu_6$=638 $cm^{-1}$ ($E_g$), $\nu_7$=196 $cm^{-1}$ ($E_g$), $\nu_8$=143 $cm^{-1}$ ($E_g$) [[16]].

In the Raman spectra of the materials under study, the bands conforming to the structure of anatase appear at a Zr/Ti ratio of up to 0.04 and a Hf/Ti ratio of up to 0.06 (Figure 5). Figure 6 shows the dependence of the bands maxima $\nu_4$, $\nu_6$, $\nu_8$ in the spectra on the Zr/Ti ratio (0 – 0.04) and Hf/Ti ratio (0 – 0.06). Along with the increase in the content of the dopant, a shift of the bands $\nu_4$, $\nu_6$ and $\nu_8$ towards lower frequencies is observed.

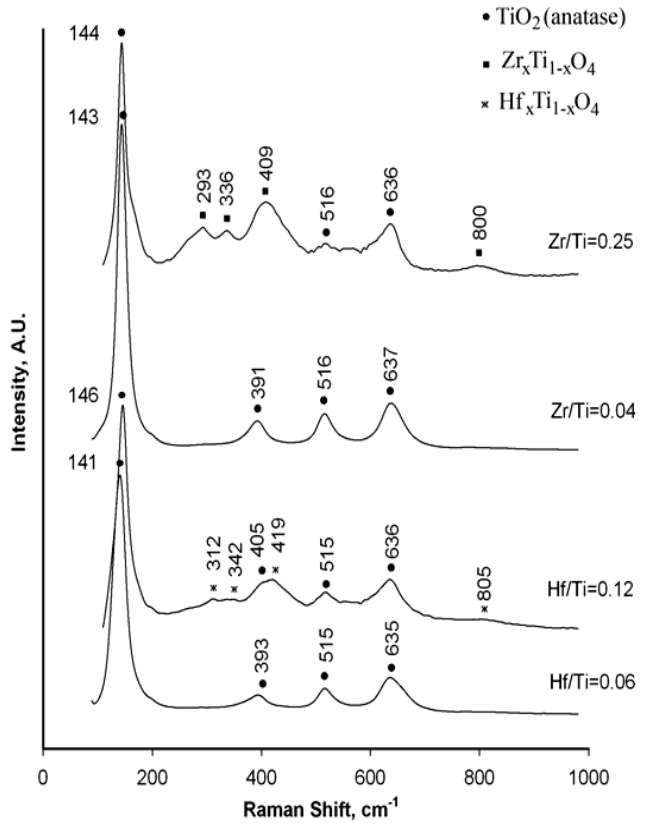


**Figure 5.** Raman spectra of the $TiO_2/ZrO_2$ (a) and $TiO_2/HfO_2$ (b) annealed at 650°C.

A number of studies of the reasons of the bands' location change in the Raman spectra of nanosized materials were performed [[17], [18], [19]]. The nanocrystallite size change was identified

as the main reason of the above processes. As was shown on the example of nanodispersed $TiO_2$ (anatase), low-frequency shift of bands in the spectrum was observed along with the increase of the sizes of nanocrystallites [[17]]. According to the data of SAXS (Figure 4) and Raman spectroscopy, the above-mentioned dependence is not valid for materials examined in the present paper.

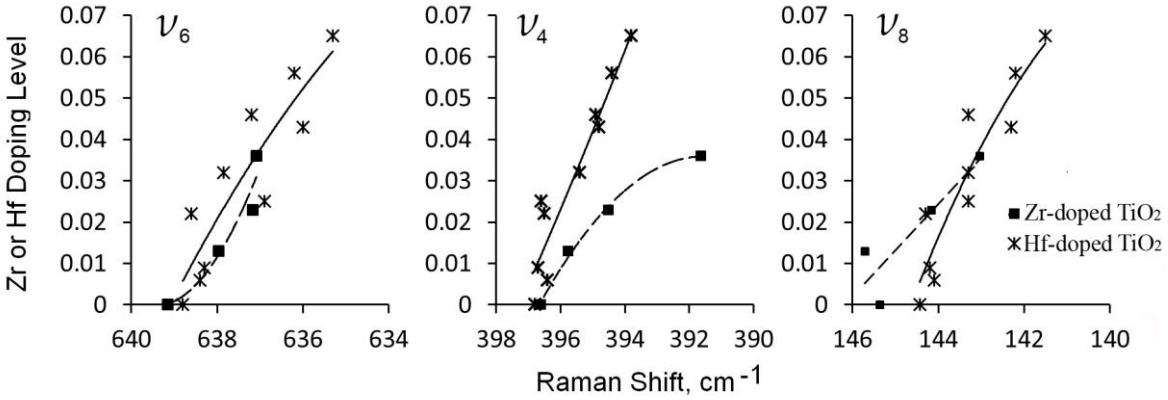


**Figure 6.** Dependence of bands maxima positions in the Raman spectra on the doping level.

It is generally accepted that the other cause of the low-frequency shift of the $\nu_4$, $\nu_6$, $\nu_8$ bands in the spectra is related to the presence of structural defects [[18], [19]], which can include incorporation of the dopant atoms into the material structure that results in changes of lattice parameters. In the spectra of Zr-doped materials, the more noticeable shift of the $\nu_4$ band (as compared to that of Hf-doped materials) was observed (Figure 6). Taking into account similarity of the $Zr^{4+}$ and $Hf^{4+}$ ionic radii, the different behavior of the bands in the spectra can be related to the difference of their atomic masses and the emergence of the relativistic effect for hafnium. The dependence of the bands' locations on the atomic masses of cations was demonstrated on the example of spectra of $ZrO_2$ and $HfO_2$ crystals [[20]].

Thus, according to the data of Raman spectroscopy and SAXS, the materials within the range of 0-0.04 for Zr/Ti ratio and 0-0.06 for Hf/Ti ratio consist of the $Ti_{1-x}Zr_xO_2$ or $Ti_{1-x}Hf_xO_2$ nanoparticles and have the structure of anatase. Further increase of the dopant contents in the studied materials results in changes in the Raman spectra. In addition to bands of anatase, the bands corresponding to the phase of zirconium or hafnium titanate emerge (Figure 5) [[21]]. Therefore, one can assume the formation, along with the increase of the doping level (Zr/Ti>0.04 and Hf/Ti>0.06), of nanoparticles having a core (nanocrystallite) composed of solid solutions of $Ti_{1-x}Zr_xO_2$ or $Ti_{1-x}Hf_xO_2$ with the anatase structure and a shell consisted of both anatase and zirconium or hafnium titanate. The emergence of the second maximum on the *P(r)* curve (Figure 3b) and changes in the Raman spectra (Figure 5) are in agreement with this assumption. According to the SAXS data, the shell growth takes place along with increase in the doping level. i.e., in changes of the maxima ratio on the *P(r)* curve changes. These conclusions agree well with different temperatures of crystallization of tentative structural components, since crystallization of the undoped $TiO_2$ can occur in the range 250-500°C while crystallization of $ZrTiO_4$ – in the range 600–1300°C depending on preparation conditions [[14], [22]].

*3.4. Electrochemical investigations*

To evaluate the electrochemical performance of nanostructured Zr- and Hf-doped anatase $TiO_2$ materials as anodes for Li-ion batteries, preliminary galvanostatic discharge–charge measurements were carried out. Figure 1 shows the results of 20-fold cycling for undoped, Zr-doped (Zr/Ti = 0.01; 0.02; 0.03), and Hf-doped (Hf/Ti = 0.01; 0.02; 0.04; 0.06) anatase $TiO_2$ electrodes at a 0.1*C*-rate.

The reversible capacities of nanostructured $Ti_{0.99}Zr_{0.01}O_2$, $Ti_{0.98}Zr_{0.02}O_2$, and $Ti_{0.97}Zr_{0.03}O_2$ are 80, 95, and 140 mAh $g^{-1}$, respectively, demonstrating better capacity retention of the doped electrodes in comparison with undoped $TiO_2$ that yielded only 65 mAh $g^{-1}$. It seems that enhanced capacities of doped samples are mainly related to facilitating of $Li^+$ ions diffusion due to the difference in the values of ionic radii of $Zr^{4+}$ and $Ti^{4+}$ ions leading to changes in lattice parameters of anatase $TiO_2$. In addition, according to electrochemical impedance spectroscopy, the charge redistribution in Zr-doped $TiO_2$ lattice results in the conductivity increase by two orders of magnitude from $4.4 \cdot 10^{-11}$ S $cm^{-1}$ (undoped) to $2.2 \cdot 10^{-9}$ S $cm^{-1}$ (Zr/Ti = 0.03) that promotes the electron transport [[23]].

The reversible capacities of nanostructured $Ti_{0.99}Hf_{0.01}O_2$, $Ti_{0.98}Hf_{0.02}O_2$, $Ti_{0.96}Hf_{0.04}O_2$, and $Ti_{0.94}Hf_{0.06}O_2$ are found to be equal to 50, 45, 85, and 55 mAh $g^{-1}$, respectively, which are some lower in comparison with Zr-doped $TiO_2$. Furthermore, the capacity dependence on the Hf concentration is not linear in contrast to Zr. The best result was observed for $Ti_{0.96}Hf_{0.04}O_2$. The electrochemical behavior of the doped $TiO_2$ is directly depends on the particle size distribution, parameters of the crystal lattice, the number of oxygen vacancies, etc. So we suggest that the inferior capacity enhancement for Hf-doped $TiO_2$ (as compared to Zr-doped one) is the effect of larger nanoparticles (Figure 7).

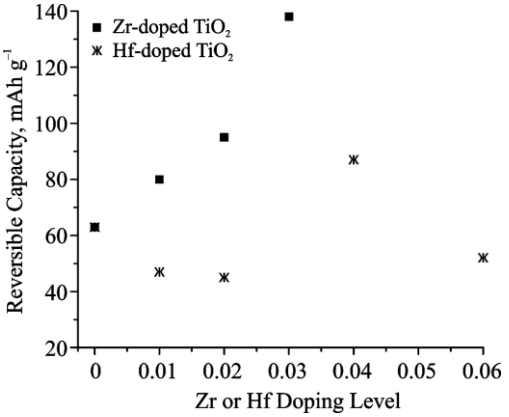


**Figure 7.** Dependence of reversible capacity after the 20-fold cycling on the doping level.

Note that $ZrTiO_4$ and $HfTiO_4$) are electric insulators [[24]]. Hence the formation of $Zr_{1-x}Ti_xO_4$ (or $Hf_{1-x}Ti_xO_4$) solid solution deteriorates the conductivity of the doped material leading to inferior electrochemical parameters of its application as Li-ion battery anode.

## 4. Conclusions

New $TiO_2/ZrO_2$ and $TiO_2/HfO_2$ materials of varying compositions have been fabricated by the template sol-gel method. The oxides consist of nanostructured microsized tubes formed by nanoparticles of sizes varying from 15 to 50 nm. $TiO_2$-based Hf-doped microtubes have larger diameters and consist of larger nanoparticles as compared to Zr-doped ones.

In the ranges of 0 to 0.04 for the Zr/Ti ratio and 0 to 0.06 for the Hf/Ti ratio, the materials are formed by nanoparticles composed of $Ti_{1-x}Zr_xO_2$ or $Ti_{1-x}Hf_xO_2$ and have the structure of anatase.

The increase in the material doping level above 0.04 (Zr/Ti) and 0.06 (Hf/Ti) yields changes in the structure of nanoparticles. Probably, the nanoparticles have a core (nanocrystallite) formed by solid solutions of $Ti_{1-x}Zr_xO_2$ or $Ti_{1-x}Hf_xO_2$ with the anatase structure and a shell consisted of both anatase and $Zr_xTi_{1-x}O_4$ or $Hf_xTi_{1-x}O_4$ at the above-mentioned content of dopants.

The promising electrochemical properties of both as-prepared Zr- and Hf-doped anatase $TiO_2$ samples as anodes for Li-ion batteries were identified. A good reversibility of the $Li^+$ intercalation into and deintercalation from the nanostructured Zr- and Hf-doped $TiO_2$ results from lattice parameters changes and conductivity increase and, thus, provides the improved dynamics for both electron and ion transport. To sum up, the method of synthesis is efficient in terms of the electrochemical performance of the battery systems.

**Acknowledgements**

The synthesis and study of the materials' morphology and structure were carried out under the program of fundamental scientific research of the Russian Academy of Sciences (project No. 0265-2014-0001, the Federal Agency of Scientific Organizations).

The electrochemical studies were carried out with the support of the Russian Science Foundation (project No. 14-33-00009) and the Government of the Russian Federation (the Federal Agency of Scientific Organizations).

**References**

[1] Kubacka A, Fernández-García M and Colón G 2012 Ch*em. Rev.* **112** 1555–614

[2] Wang X, Li Z, Shi J and Yu Y 2014 *Chem. Rev*. **114** 9346-84

[3] Bai Y, Mora-Seró I, De Angelis F, Bisquert J and Wang P 2014 *Chem. Rev*. **114** 10095−130

[4] Reddy B M and Khan A 2005 *Catalysis Reviews* **47** 257–96

[5] Ma Y, Wang X, Jia Y, Chen X Han H and Li C 2014 *Chem. Rev*. **114** 9987−10043

[6] Macwan D P, Dave P N 2011 *J. Mater. Sci*. **46** 3669–86

[7] Cargnello M, Gordon T R and Murray C B 2014 *Chem. Rev*. **114** 9319−45

[8] Schneider J, Matsuoka M, Takeuchi M, Zhang J, Horiuchi Y, Anpo M and Bahnemann DW. 2014 *Chem. Rev*. **114** 9919−86

[9] Betenekov N D, Vasilevskij V A, Egorov Yu V and Nedobukh T A 1982 Radiokhimiya **24** 419–24 (Russ)

[10] Gnedenkov S V, Opra D P, Sinebryukhov S L, Kuryavyi V G, Ustinov A Yu and Sergienko V I 2015 *J. Alloy. Compd*. **621** 364

[11] Sinebryukhov S L. Opra D P, Gnedenkov S V, Minaev A N, Sokolov A A, Kuryavyi V G and Zheleznov V V 2015 *Int. Ocean and Polar Eng.* **1** 621

[12] Gnedenkov S V, Opra D P, Kuryavyi V G, Sinebryukhov S L, Ustinov A Yu and Sergienko V I 2015 *Nanotechnol.* **10** 353 (Russ)

[13] Semenyuk A V and Svergun D I 1991 *J. Appl. Cryst*. **24** 5 537–40

[14] Chang S M and Doong R M 2006 *J. Phys. Chem. B* **110** 20808–14

[15] Balmer J A, Mykhaylyk O O, Schmid A, Armes S P, Fairclough J P A and Ryan A J |2011 *Langmuir* **27** 8075–89

[16] Ohsaka T, Izumi F and Fujiki Y J 1978 *J. Raman spectrosc*. **7** 321–24

[17] Wang D, Chen B and Zhao J 2007 *J. Appl. Phys.* 101 113501-113501-5

[18] Gupta S K, Desai R, Jha P K, Sahoob S and Kirinc D 2010 *J. Raman Spectrosc.* **41** 350–55

[19] Parker J C and Siegel R W 1990 *J. Appl. Phys.* **57** 943

[20] Haines J and Le´ger J M, Hull S, Petitet J P, Pereira A S, Perottoni C A and da Jornada J A H 1997 *J. Am. Ceram. Soc.* **80** 1910–14

[21] Krebs M A and Condrate R A 1988 *J. Mater. Sci. Lett*. **7** 1327–30

[22] Dos Santos V, Zeni M, Hohemberger J M, and Bergmann C P 2010 *Rev. Adv. Mater. Sci.* **24** 44

[23] Opra D P, Gnedenkov S V, Sokolov A A, Zheleznov V V, Voit E I, Sushkov Yu V and Sinebryukhov S L 2015 *Scripta Mater.* **107** 136

[24] Vittayakorn N 2006 *J. Ceram. Process. Res.* **7** 288–91